INTERNATIONAL JOURNAL FOR NUMERICAL METHODS IN FLUIDS, VOL. 8, 1011–1027 (1988)

THE FREE SURFACE FLOW OF NEWTONIAN AND NON-NEWTONIAN FLUIDS TRAPPED BY SURFACE TENSION

D. M. TIDD

Naval Architects and Future Projects Department, Vickers Shipbuilding and Engineering Ltd., Barrow-in-Furness, Cumbria LA14 1AF, U.K.

R. W. THATCHER AND A. KAYE

Department of Mathematics, University of Manchester Institute of Science and Technology, P.O. Box 88, Manchester M60 1QD, U.K.

SUMMARY

In this paper the position of the free surface of a swirling fluid held in by surface tension is calculated by the finite element method. A new locally mass-conserving quadratic velocity, linear pressure triangular element is used to overcome non-physical solutions produced by the well known Taylor–Hood element.

KEY WORDS Free Surface Finite Element Method Surface Tension Newtonian and Non-Newtonian Fluids

1. INTRODUCTION

This paper is concerned with finding the shape of a free surface and calculating the flow pattern of Newtonian and non-Newtonian fluids. We first consider the case of fluid confined by surface tension between two finite parallel plates rotating with different angular velocities. Secondly we consider the case where the top plate is replaced by a cone whose vertex touches the centre of the bottom plate.

For in finite rotating parallel plates, where there are no complications caused by the free surface, an 'exact' solution exists for a Newtonian fluid. A similarity transformation is applied to the Navier–Stokes equations, reducing them to a set of ordinary differential equations. There are several publications giving solutions for increasing Reynolds number; see e.g. Holodniok *et al.*[1] Pao[2] first investigated the flow between finite parallel plates enclosed by a cylinder of aspect ratio (defined as cylinder height divided by plate radius) unity. Dijkstra and van Heijst[3] obtain results both experimentally and numerically for this flow with a smaller aspect ratio. In their configuration the cylinder rotates with the bottom plate, giving a singularity where the top plate meets the cylinder.

The finite geometries discussed in this paper model the flow in two types of rheogoniometer which are used to measure and gain insight into the rheological properties of fluids. A frequently used approximation in the literature is that the inertial effects are neglected, i.e. fluid is assumed to flow in a simple primary pattern. However, secondary flow in the cone–plate geometry was observed as early as 1962 by Cox.[4] Since that time there have been many publications on numerical and experimental techniques to calculate the effects of the secondary flow (see e.g. the review in Walters[5]). However, most of these neglect the effects of the free surface at the liquid/air

0271–2091/88/091011–17$08.50

Received 8 December 1986
Revised 8 December 1987

interface. The apparatus is either assumed to be in a sea of liquid or the free surface is assumed to remain in its unperturbed state. Two exceptions to this are the free surface calculations of Joseph[6] and of Harriott and Brown[7] for Newtonian fluids in the parallel plate geometry.

Free surface problems with surface tension are known to be a difficult numerical problem. Tanner *et al.*[8] among others have computed the flow of a free viscous jet where surface tension effects have been taken into account. They report that the solution convergence is more limited by surface tension than by Reynolds number and as a result it is more difficult to establish the effect of high surface tension on jet shape. They were primarily concerned with the die swell phenomenon and the extensions to non-Newtonian fluids. The surface tension in their jet problem is not as important as in the case considered here, where the fluid is completely held in by surface tension effects.

Ruschak and Scriven[9] have presented results for two-dimensional flow of a Newtonian liquid coating a rotating horizontal cylinder. They consider the perturbation from the rigid body solution which is obtained when gravity is zero, Orr and Scriven[10] develop this further by using the finite element method to solve the equations directly. Locating the free surface is found to be difficult, particularly when surface tension is high, but they manage to develop a scheme using the normal stress condition to move the boundary and having the remaining free surface conditions satisfied by the finite element algorithm.

Hyun[11] has investigated the flow of an incompressive fluid inside a cylinder driven by a spinning bottom. The character of the flow changed depending on whether free surface conditions or rigid wall conditions were imposed on the top surface, particularly when the aspect ratio (cylinder height/radius) was small. A horizontal approximation to the free surface position was used and no attempt to find the exact free surface position was made. Keunings[12] has investigated some transient free surface problems for non-Newtonian fluids.

In the next two sections we deal with a Newtonian fluid for our two configurations outlined above. In Section 2 we set up the parallel plate model and simplify the Navier–Stokes equations by considering an expansion of the pressure and velocity variables in terms of the angular velocity Ω. The resulting system is solved using the finite element method in a rectangular region using three of the four boundary conditions on the free surface. The free surface is then calculated using the remaining boundary condition together with the requirement that the volume of the trapped fluid is conserved. This perturbation approach to the problem is similar to that used by Joseph[6] and by Harriott and Brown.[7] In Section 3 we solve a similar set of equations for the cone and plate model in a triangular region. Finally in Section 4 we set up some non-Newtonian fluid equations equivalent to those in the first two sections and outline our investigations in this area.

For the non-Newtonian flow the choice of a triangular finite element has a critical effect on obtaining physically meaningful solutions. In particular with quadratic velocities, changing the pressure-approximating field from continuous piecewise linear (the 'Taylor–Hood'[13] element) to one whereby continuous piecewise linear and piecewise constant pressure fields are superimposed enables us to model this type of flow.

2. NEWTONIAN FLUID BETWEEN PARALLEL PLATES

2.1. *The free surface problem*

Our aim is to model the particular fluid measuring device illustrated in Figure 1. The device consists of two parallel circular plates of radius a and distance h apart, with h very much smaller than a. A pipe is connected to the centre of the bottom plate to allow fluid into the device or equivalently to vary the pressure at this point. A Newtonian incompressible liquid of viscosity μ

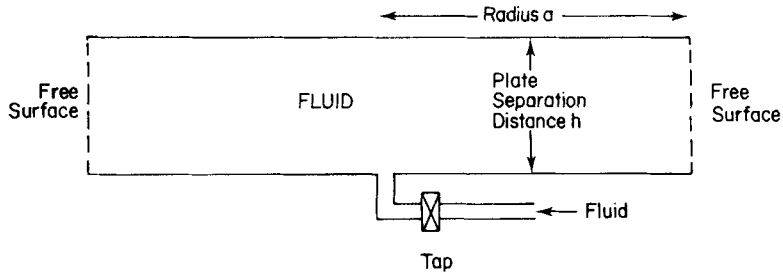

Figure 1. The physical problem

and density ρ is held between the plates by surface tension at the free surface. The shape of the free surface is altered by rotating the two plates at different angular velocities about their centres. We consider various choices of the parameters K ($|K| \leqslant 1$) and L ($|L| \leqslant 1$), where $K\Omega$ is the angular velocity of the top plate and $L\Omega$ is the angular velocity of the bottom plate.

The governing system of non-linear partial differential equations in the interior of the region defined by Figure 2 is given by the Navier–Stokes equations and the continuity equation, both in cylindrical polar co-ordinates. We ignore gravitational effects, which are small since the distance h is small. We also assume that the fluid is in a steady state with axial symmetry. The boundary conditions are no slip on the top and bottom plate with symmetry conditions on the centreline. On the free surface we require (see Tidd *et al.*[14] or Jeseph[6] for further details) no normal velocity and there are three stress boundary conditions, which may be written as

$$P_{r\theta} + P_{\theta z} \tan\psi = 0, \tag{1}$$

$$(1 - \tan^2\psi) P_{rz} + (P_{zz} - P_{rr}) \tan\psi = 0 \tag{2}$$

and

$$P_{rr} + P_{zz} \tan^2\psi + 2P_{rz} \tan\psi = T\left(\frac{d^2r/dz^2}{[1+(dr/dz)^2]^{1/2}} - \frac{[1+(dr/dz)^2]^{1/2}}{r} \right), \tag{3}$$

where P_{rr}, P_{zz}, P_{rz}, $P_{r\theta}$ and $P_{\theta z}$ are the components of the stress tensor in the appropriate directions and may be expressed in terms of the radial, tangential and axial velocities u, v, w and the pressure P.

For the trivial case of $\Omega = 0$, where there is no flow and the pressure is constant, the free surface boundary conditions reduce to an ordinary differential equation in the free surface position $f(z)$. If

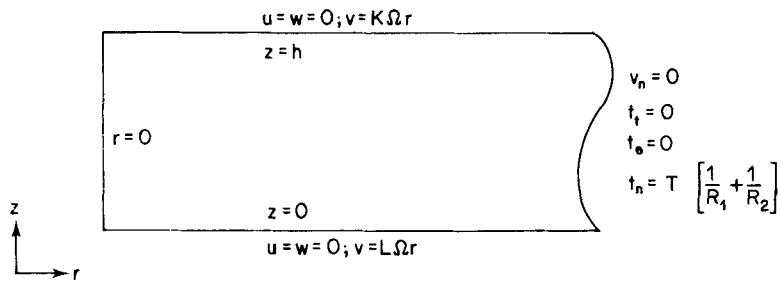

Figure 2. Boundary conditions for parallel plate geometry

we vary the pressure we obtain different profiles for the free surface. A value of $P = T/a$ gives us a free surface which is a cylinder.

2.2. *Mathematical formulation*

Following the perturbation techniques of Joseph[6] and of Harriott and Brown[7], a series solution in powers of Ω is sought in which we put

$$\begin{aligned} f(z) &= a + \Omega^2 f_2(z) + \Omega^4 f_4(z) + \ldots, \\ u &= \Omega^2 u_2 + \Omega^4 u_4 + \ldots, \\ v &= \Omega v_1 + \Omega^3 v_3 + \ldots, \\ w &= \Omega^2 w_2 + \Omega^4 w_4 + \ldots, \\ P &= P_0 + \Omega^2 P_2 + \Omega^4 P_4 + \ldots. \end{aligned}$$

The equations obtained by taking terms in Ω^0, Ω^1 and Ω^2 respectively can be written as (see Tidd *et al.*[14])

(i) $$P = P_0 = T/a, \tag{4}$$

(ii) $$\frac{\partial^2 v_1}{\partial r^2} + \frac{\partial^2 v_1}{\partial z^2} + \frac{1}{r}\frac{\partial v_1}{\partial r} - \frac{v_1}{r^2} = 0, \tag{5}$$

$$f(z) = a, \tag{6}$$

$$\frac{\partial v_1}{\partial r} - \frac{v_1}{r} = 0 \quad \text{on} \quad r = a. \tag{7}$$

The solution for v_1 is easily seen to be given by

$$v_1 = r[L + z(K - L)/h]. \tag{8}$$

(iii) $$0 = \frac{\partial u_2}{\partial r} + \frac{u_2}{r} + \frac{\partial w_2}{\partial z}, \tag{9}$$

$$-r\left(L + \frac{z(K-L)}{h}\right)^2 \equiv \frac{v_1^2}{r} = -\frac{1}{\rho}\frac{\partial P_2}{\partial r} + \frac{\mu}{\rho}\left(\frac{\partial^2 u_2}{\partial r^2} + \frac{\partial^2 u_2}{\partial z^2} + \frac{1}{r}\frac{\partial u_2}{\partial r} - \frac{u_2}{r^2}\right), \tag{10}$$

$$0 = -\frac{1}{\rho}\frac{\partial P_2}{\partial z} + \frac{\mu}{\rho}\left(\frac{\partial^2 w_2}{\partial r^2} + \frac{\partial^2 w_2}{\partial z^2} + \frac{1}{r}\frac{\partial w_2}{\partial r}\right). \tag{11}$$

In addition there are no-slip boundary conditions on the upper and lower plate and symmetry conditions on the centreline. On the free surface $r = a$ the boundary conditions are

$$u_2 = 0, \qquad \partial w_2/\partial r = 0, \tag{12}$$

$$-P_2 + \frac{2\mu \partial u_2}{\partial r} = T\left(\frac{\mathrm{d}^2 f_2(z)}{\mathrm{d}z^2} + \frac{1}{a^2} f_2(z)\right) \quad \text{on} \quad r = a,\ 0 < z < h. \tag{13}$$

The numerical solution procedure described in the next subsection amounts to solving the above equations by the finite element method with all the boundary conditions except (13). The value of P_2 is only determined up to a constant by these equations. This constant together with the free surface can then be calculated by using the condition (13) together with the requirement that volume is preserved.

2.3. *Numerical formulation*

The use of finite element procedures for fluid flow problems is well documented elsewhere; see e.g. Taylor and Hughes[15] or Teman.[16] We shall only discuss the points of particular relevance to our equations developed in Sections 2.1 and 2.2.

Following classical Galerkin weighted residual methods, we may satisfy the derivative boundary conditions as natural conditions. We then split our domain into rectangles, each in turn subdivided into two triangles, and impose the essential velocity conditions. In this paper we compare results using two triangular finite elements. The first element (element L3) is a commonly used six-noded element with nodes at the vertices and midsides.[16] The velocities are approximated locally over an element as continuous quadratic functions and the pressures as continuous linear functions. The second element (element LC) to our knowledge has not been used before and is a seven-noded element with an additional node to element L3 located at the centroid. The velocity approximation is identical to that of element L3. However, the pressure approximation is obtained by superimposing the continuous linear pressure approximation with a piecewise constant pressure field. The latter element was first suggested by Griffiths[17] in a paper discussing pressure approximations for incompressible flows. Gresho *et al.*[18] have successfully used an equivalent superposition of pressure fields for Boussinesq fluids using quadrilateral elements. They report that there is some evidence that the lack of element mass balance can lead to non-physical solutions for some problems and our evidence seems to confirm this. The element LC gives us continuity over each element whereas element L3 only ensures continuity over the domain. This element has been analysed by Thatcher and Silvester[19] and shown to satisfy the Babuska–Brezzi stability condition (see Girault and Raviart[20] for details of this condition). Moreover, they show that for the particular test problem presented it gives better answers than the similar but more complicated bubble element of Crouzeix and Raviart.

A feature of our investigations to date are the fine grids that are needed in order to achieve reasonable accuracy, particularly near the free surface. The 16×8 grid (GRID1) is illustrated in Figure 3 and is graded by constructing lines parallel to the z-axis at distances r_i, $0 \leqslant i \leqslant 16$, in the r-direction, where for fixed $\lambda < 1$

$$r_0 = 0, \qquad r_{16} = a, \qquad r_i = \lambda(r_{i-1} - r_{i-2}) + r_{i-1}; \quad 1 \leqslant i \leqslant 15.$$

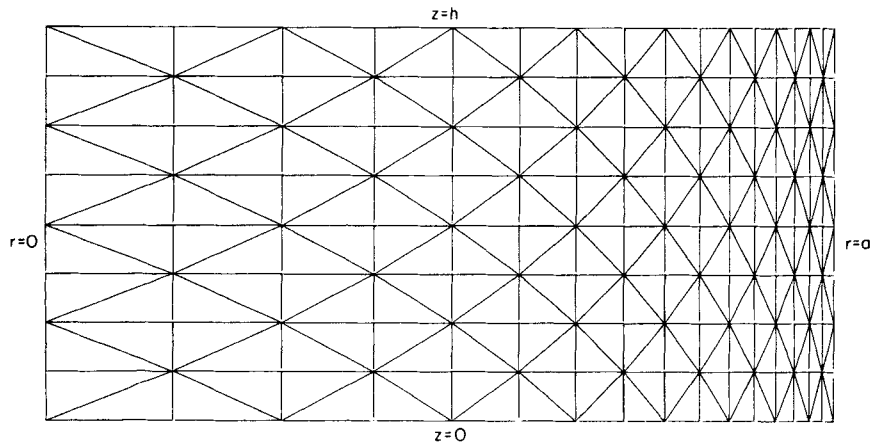

Figure 3. 16×8 graded grid (GRID1)

GRID1 is obtained by taking $\lambda = 0{\cdot}85$, but no attempt to optimize this parameter has been made. This grid is then uniformly refined to obtain a 32×16 grid (GRID2) by splitting each rectangle into four and triangulating using the same strategy as in GRID1. A 64×32 grid (GRID3) is similarly obtained from a uniform refinement of GRID2. The computer software used was based on the programs developed by Silvester.[21]

Having obtained solutions of velocities and pressures from the finite element approach, we then solve (13) to obtain f_2. From the continuity equation (9) we may use values of $-\mathrm{d}w_2/\mathrm{d}z$ for the term containing $\mathrm{d}u_2/\mathrm{d}r$ in (13). The values of $\mathrm{d}w_2/\mathrm{d}z$ may be calculated either from the finite element approximation in each element or by fitting another interpolatory function to the values of w_2. We present results using cubic splines to fit these values, which seemed to yield more satisfactory results than using the finite element approximation directly. We solved equation (13) by a finite difference technique, where the step length was determined by the finite element grid (i.e. $h/2NZ$ on an $NR \times NZ$ grid). A solution was found that insured the volume of fluid had remained constant. This was achieved by altering the value of P_2 which, as remarked above, is only determined up to a constant over the domain.

To non-dimensionalise our model we make our length, velocity and stress variables dimensionless by the use of a, $a\Omega$ and T/a respectively. Thus we use a length ratio $D = h/a$, a Reynolds number $Re = \rho\Omega a^2/\mu$ and a surface tension parameter $S = T\rho a/\mu^2$. The results we present in the next subsection all use values of $D = 0{\cdot}1$, $Re = 10{\cdot}0$ and $S = 300{\cdot}0$. Thus the numerical procedures are carried out on the rectangular domain $0 \leqslant r \leqslant 1$, $0 \leqslant z \leqslant 0{\cdot}1$. In the results it is the dimensionless forms of the variables (and equations) that are referenced.

2.4. *Results*

$K = 1, L = 1$. The simplest case is when both plates are spinning at the same rate. In this case the solution of (8)–(11) can easily be calculated and is given by

$$v_1 = r, \qquad u_2 = 0, \qquad w_2 = 0, \qquad P_2 = Re^2 r^2/2S + \text{constant}.$$

Our numerical procedures give us a solution that converges to this analytic solution as we refine the grid. The numerical solution produces larger values of u_2 compared with w_2 and these are greatest near the centreline. The critical effects of this will be seen in Section 4. For element L3 on GRID1 our numerical solution gives values of u_2 of at most 6×10^{-5} and a value of P_2 which deviates from the exact solution by 1×10^{-3}. For GRID2 these values are about 3×10^{-5} and 2×10^{-4} respectively. For element LC the results for u_2 annd w_2 are more accurate, giving approximately a factor of ten improvement on their respective largest values. The pressure deviation from the exact solution is, however, approximately the same as with element L3. The free surface, i.e. f_2, from equation (13) is given by $f_2 = 0$ and the actual value of P_2 here is zero on the free surface, thus determining the constant above.

$K = 1$, $0 \leqslant L < 1$. For this case the acceleration terms in the equations generate a radial flow which will be 'out' at the top and 'in' at the bottom. This will bulge the free surface and our aim is to calculate the profile of this bulge given by f_2. The numerical values of w_2 obtained on the free surface agree to two significant figures from one grid to the next. The values for element LC are more accurate than those obtained using element L3 with three figures of agreement from GRID2 to GRID3. The values of w_2 for $0 \leqslant r \leqslant 0{\cdot}9$ are ten times smaller than those on the free surface, and the solution shows more significant figures of agreement from one grid to the next at points away from the free surface. For the case of two infinite plates rotating the axial velocity is independent of radial position. Our values of w_2 are in agreement with this away from the free surface for r approximately in the range $0 \leqslant r \leqslant 0{\cdot}8$. The directions of u_2 and w_2 and associated streamline

pattern are illustrated in Figures 4 and 5 respectively. The free surface positions, f_2, are given in Table I, where again the LC element results appear more accurate than the L3 element results.

The same series expansion has been carried out by Kaye[22] for the case of infinite plates with $K=1$, $L=0$. It is shown that the pressure p^{I} on the lower plate is given by

$$p^{\mathrm{I}}=p_0^{\mathrm{I}}+\Omega^2 Cr^2 \tag{14}$$

where for this case $C=0{\cdot}05$ and the value of p_0^{I} is indeterminate. It is interesting to compare these pressure results with those that we have obtained, namely

$$P(r, z)=1+\Omega^2 P_2(r, z) \tag{15}$$

and in particular to compare $P_2(r, 0)$ on GRID3 with Cr^2. However, the effect of the free surface makes the value of $P_2(0, 0)$ $-0{\cdot}050014$ on GRID3 for element L3. In Table II we compare the values of Cr^2 with $P_2(r, 0)-P_2(0, 0)$ along the lower plate. It is noted that these values compare

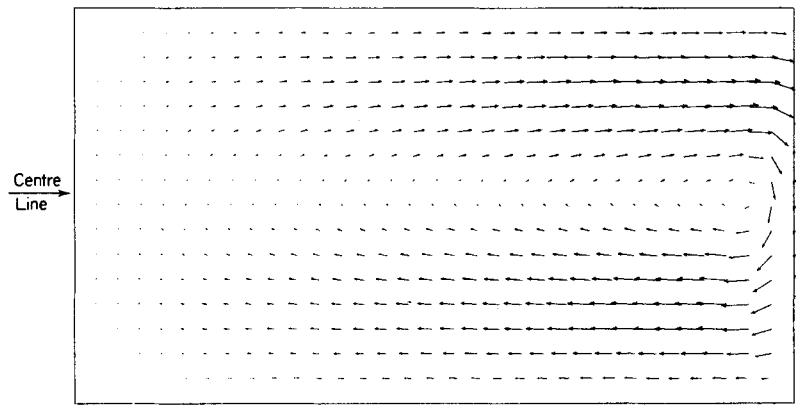

Figure 4. Parallel plate flow pattern for $K=1$, $L=0$ with $Re=10$. Note: size of arrows reflects speed of flow

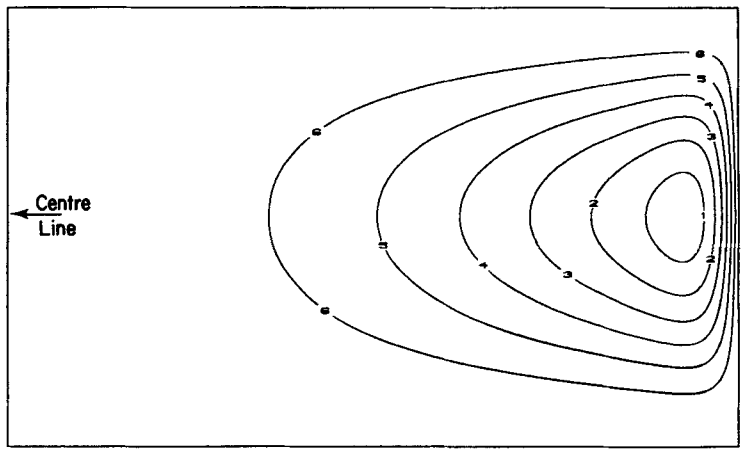

Figure 5. Parallel plate streamlines for $K=1$, $L=0$ with $Re=10$. Contour values: 1, $-0{\cdot}22$E-4; 2, $-0{\cdot}18$E-4; 3, $-0{\cdot}14$E-4; 4, $-0{\cdot}1$E-4; 5, $-0{\cdot}7$E-5; 6, $-0{\cdot}4$E-5

Table I. Parallel plates. Values of f_2 for $Re=10$ with $K=1$, $L=0$ (in units of 10^{-6})

	Element L3			Element LC		
z	GRID1	GRID2	GRID3	GRID1	GRID2	GRID3
0·0125	−0·5943	−0·5990	−0·6002	−0·5982	−0·6001	−0·6004
0·025	−0·7964	−0·8019	−0·8035	−0·8014	−0·8031	−0·8036
0·0375	−0·5814	−0·5853	−0·5867	−0·5845	−0·5863	−0·5868
0·05	−0·0752	−0·0772	−0·0778	−0·0755	−0·0773	−0·0777
0·0625	0·4904	0·4921	0·4926	0·4940	0·4929	0·4928
0·075	0·8370	0·8414	0·8427	0·8436	0·8429	0·8431
0·0875	0·7069	0·7126	0·7142	0·7122	0·7144	0·7146

Table II. Values of $P_2(r,0)-P_2(0,0)$ on GRID3 and Cr^2 on the lower disc for $Re=10$ with $K=1$, $L=0$

r	Parallel plates $P_2(r,0)-P_2(0,0)$	Kaye[22] Cr^2	Cone and plate $P_2(r,0)-P_2(0,0)$
0·0	0·0	0·0	0·0
0·2997	0·004501	0·004491	0·004357
0·5163	0·013342	0·013328	0·013125
0·6728	0·022649	0·022633	0·022354
0·7858	0·030891	0·030874	0·030527
0·8675	0·037652	0·037628	0·037230
0·9265	0·043068	0·042920	0·042611
0·9691	0·047149	0·046958	0·046756
1·0	0·048801	0·050000	0·048473

well, particularly away from the free surface. Thus the use of the infinite plate to calculate pressures on the lower plate gives errors of the order $\Omega^2 P_2(0,0)$.

The recirculation that can be seen in Figures 4 and 5 moves slightly nearer the lower plate if the lower plate is spun with L in the range $0<L<1$, disappearing when $L=1$. The free surface shapes for $K=1$ with $L=0$ and $L=0{\cdot}5$ are illustrated in Figure 6.

$K=1$, $-1\leqslant L<0$. In the situation of the top plate rotating in the opposite direction to the lower plate at an equal rate ($K=1$, $L=-1$), two recirculations are set up. The solution is, as expected, symmetric to numerical accuracy; the streamlines for this case are illustrated in Figure 7. The free surface is also symmetric and shows a 'bulge out' near each plate and a 'bulge inwards' in the centre.

The second recirculation is not resolved by our grids for $K=1$, $-0{\cdot}5<L<0$ but evidence of it can be seen on the finer grids at a few points for $L=-0{\cdot}5$. The streamlines for the case $K=1$, $L=-0{\cdot}75$, showing the second recirculation, are illustrated in Figure 8. The dividing streamline $\phi=0$ starts on the centreline and ends on the free surface, forming a stagnation point near $r=a$ where the effect of the slower rotating disc is largest. The free surface shapes for $K=1$ with $L=-0{\cdot}5$, $L=-0{\cdot}75$ and $L=-1$ are illustrated in Figure 9.

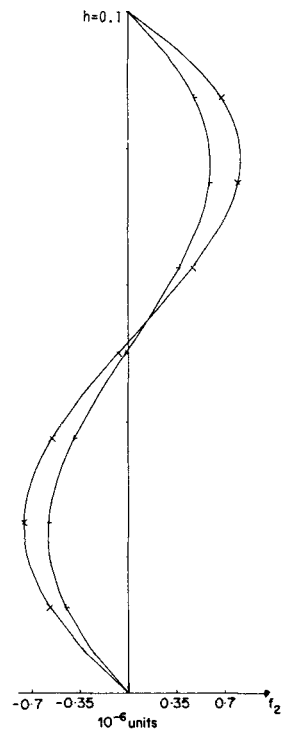

Figure 6. Parallel plate free surface shapes for $Re=10$: $\times$, $K=1$, $L=0$; $+$, $K=1$, $L=0{\cdot}5$

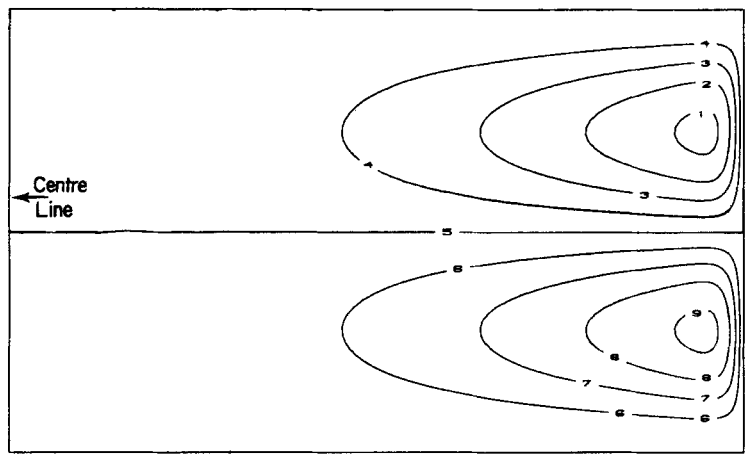

Figure 7. Parallel plate streamlines for $K=1$, $L=-1$ with $Re=10$. Contour values: 1, $-0{\cdot}54$E-5; 2, $-0{\cdot}41$E-5; 3, $-0{\cdot}27$E-5; 4, $-0{\cdot}14$E-5; 5, 0·0; 6, 0·14E-5; 7, 0·27E-5; 8, 0·41E-5; 9, 0·54E-5

2.5. *Other related published results*

The shape and position of the free surface has been calculated for low Reynolds number by Joseph[6] and by Harriott and Brown.[7] Joseph has done an asymptotic analysis for the limit of small aspect ratio and the results presented above are in qualitative agreement with these. In

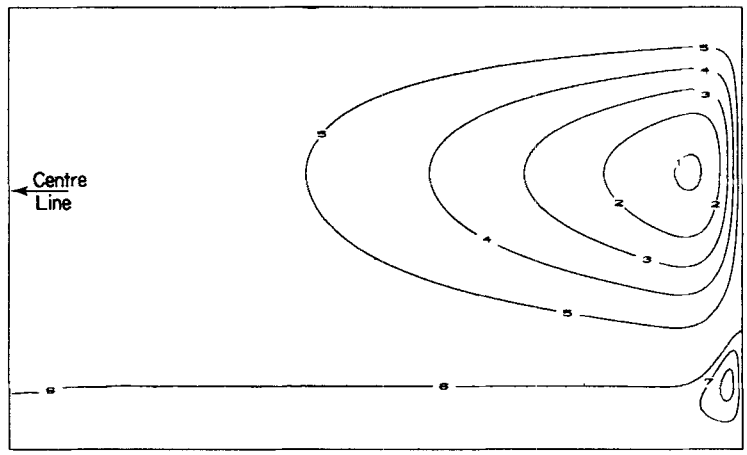

Figure 8. Parallel plate streamlines for $K=1$, $L=-0{\cdot}75$ with $Re=10$. Contour values: 1, $-0{\cdot}12$E-4; 2, $-0{\cdot}99$E-5; 3, $-0{\cdot}74$E-5; 4, $-0{\cdot}49$E-5; 5, $-0{\cdot}25$E-5; 6, 0·0; 7, 0·25E-6; 8, 0·5E-6

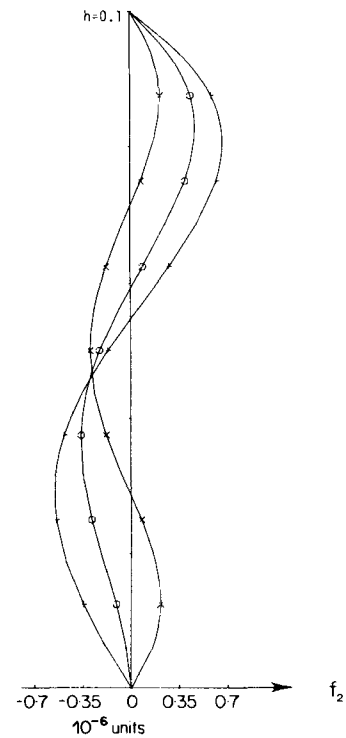

Figure 9. Parallel plate free surface shapes for $Re=10$: +, $K=1$, $L=-0{\cdot}5$; ○, $K=1$, $L=-0{\cdot}75$; ×, $K=1$, $L=-1$

particular the free surface position given in Table I agrees with the results of Joseph to one significant figure. Harriott and Brown have found a solution in the form of a series of Bessel functions by using a stream function approach to equations (9)–(11). The aspect ratios used in their paper are considerably larger (in the range $0{\cdot}2 \leqslant D \leqslant 5$) than the one used above ($D = 0{\cdot}1$), so no comparison is appropriate.

The results for $-1 \leqslant K < 0$ differ significantly from those obtained by Dijkstra and van Heijst[3] who consider the flow between finite rotating plates enclosed by a cylinder (which is rotating with the lower plate). It is not surprising that these results differ from ours because of the rotating wall, although for $K \geqslant 0$ the results are quantitatively similar. Dijkstra and van Heijst have resolved a second recirculation even for a counter-rotation factor of $-0{\cdot}3$. However, their numerical and experimental procedures fail for a counter-rotation factor of $K < -0{\cdot}825$ owing to the strong velocity singularity where the top rotating plate meets the rotating cylinder. In contrast the grids used in this paper, with the plates bounded by a free surface, have not been able to resolve a second recirculation for $-0{\cdot}5 \leqslant K < 0$. A second recirculation has been shown to develop near the free surface for $K = -0{\cdot}75$, with a fully symmetric solution reached at $K = 1$. However, these solutions are consistent with the results of Harriott and Brown.[7] For small aspect ratio and low Reynolds number they predict that two recirculations will exist for rotation ratios in the range $-1 \leqslant K \leqslant -2/3$ and that the axial location of the dividing streamline is at

$$z = -(2 + 3K)/10(1 - K). \tag{16}$$

Equation (16) is valid for radial positions away from the free surface and is in excellent agreement with the position of the dividing streamline in Figure 8.

Further comparisons of the above results with those in the literature can be found in Tidd.[23]

3. NEWTONIAN FLUID BETWEEN CONE AND PLATE

We now consider the case of the top plate being replaced by a rotating cone. We use the same values of the non-dimensional numbers defined in the previous section and hence the angle that the cone makes with the bottom plate is small. We thus expect similar results to those already given for the parallel plate model.

The equations of Section 2.1 follow through immediately, apart from the boundary conditions which are now applied on a cone-shaped region. The main difference is that it is now necessary to solve for v_1 numerically. For the solution of the cone and plate flow we first solve (5) with boundary conditions to obtain an approximation to v_1 at the grid points. For this we again use the finite element method and approximate v_1 as continuous quadratic functions over an element. We then use the calculated values of v_1 to evaluate the term containing v_1 in (10) using a three-point Gaussian quadrature rule over each element. Full solutions are then obtained as before using the same two types of element. GRID4 with 32 elements along the bottom plate and 16 elements on the free surface is illustrated in Figure 10. The grading in the radial direction of grid GRID4 is identical to that for grid GRID1 and the parameter λ was again chosen to be 0·85. Further grids doubling the number of elements in each direction were used, as before, to demonstrate convergence (viz. GRID5 and GRID6 respectively).

3.1. *Results*

The values of v_1 obtained on the three grids used proved to be fairly accurate, typically showing four significant figures of agreement from one grid to the next. The results corresponding to those of Table I are given in Table III for the cone and plate configuration with $K = 1$ and $L = 0$. Again

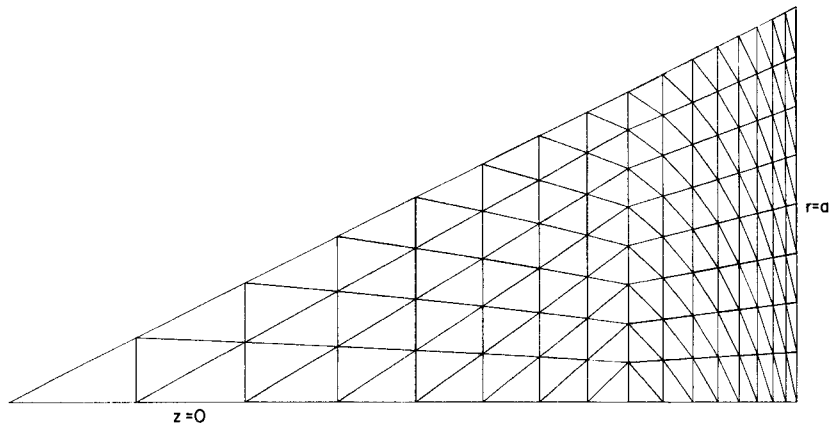

Figure 10. GRID4

Table III. Cone and plate. Values of f_2 for $Re=10$ with $K=1$, $L=0$ (in units of 10^{-6})

	Element L3			Element LC		
z	GRID1	GRID2	GRID3	GRID1	GRID2	GRID3
0·0125	−0·6043	−0·6041	−0·6043	−0·6034	−0·6041	−0·6042
0·025	−0·7965	−0·7970	−0·7975	−0·7956	−0·7970	−0·7974
0·0375	−0·5664	−0·5679	−0·5685	−0·5659	−0·5678	−0·5683
0·05	−0·0545	−0·0563	−0·0569	−0·0546	−0·0563	−0·0567
0·0625	0·5018	0·5005	0·5003	0·5010	0·5005	0·5004
0·075	0·8269	0·8266	0·8269	0·8257	0·8267	0·8270
0·0875	0·6843	0·6858	0·6863	0·6842	0·6858	0·6864

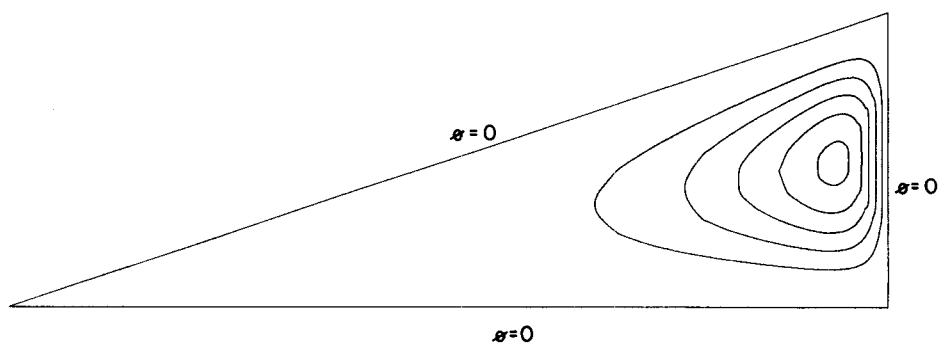

Figure 11. Cone and plate streamlines for Newtonian fluid with $K=1$, $L=0$ and $Re=10$. Contour values: −0·4E-5, −0·7E-5, −0·1E-4, −0·14E-4, −0·18E-4

element LC appears to give more accurate values of w_2 and f_2. The streamlines for this case are illustrated in Figure 11.

The case of an infinite cone and plate geometry has also been carried out by Kaye[22] for $K=1$ and $L=0$. The pressure on the lower plate is again shown to satisfy (14) and so a similar analysis

to the parallel plate geometry is valid (see Section 2.4 and Table II). The value $P_2(0, 0)$ on GRID6 for element L3 is found to be $-0{\cdot}04979$.

Two recirculations are again set up when the cone is rotated in an opposite direction to the plate ($K=1$, $L=-1$). The solution is not symmetric in this case and the recirculation near the cone surface is slightly stronger than the recirculation near the plate. For L approaching zero (with $K=1$) the lower recirculation becomes much weaker as in the parallel plate geometry.

4. NON-NEWTONIAN FLUID SOLUTIONS

In this section we calculate the flow patterns and free surface shapes for a non-Newtonian fluid in the two geometries. There are many different models of non-Newtonian fluid flow, each determined by the choice of constitutive equation. For a Newtonian fluid there is only one constitutive equation, namely

$$\mathbf{P}+p\mathbf{I}=\mu\mathbf{A}^{(1)}, \tag{17}$$

where in rectangular Cartesian co-ordinates we have: $\mathbf{P}=(P_{ij})$ is the stress tensor; $\mathbf{I}=(\delta_{ij})$ is the identity function; $\mathbf{A}^{(1)}=(A_{ij}^{(1)})$, with $A_{ij}^{(1)}=\partial v_i/\partial x_j+\partial v_j/\partial x_i$; μ is the viscosity and p is the pressure.

The choice of non-Newtonian constitutive equation adopted here is a generalization of (17) given by

$$\mathbf{P}+p\mathbf{I}=\mu_1\mathbf{A}^{(1)}+\mu_2\mathbf{A}^{(2)}+\mu_3(\mathbf{A}^{(1)})^2, \tag{18}$$

where

$$\mathbf{A}^{(2)}=(A_{ij}^{(2)})=v_k\frac{\partial A_{ij}^{(1)}}{\partial x_k}+A_{ik}^{(1)}\frac{\partial v_k}{\partial x_j}+A_{kj}^{(1)}\frac{\partial v_k}{\partial x_i}$$

and μ_1, μ_2, μ_3 are constants.

The constitutive equation (18) is of the Rivlin–Ericksen type and generally used in problems where the velocities are small. For our purposes we assume the velocities are small in order to obtain a perturbation solution to the equations of motion in a manner similar to those in Sections 2 and 3. An approximate relation between μ_2 and μ_3 exists given by (see Bird *et al.*[24])

$$2\mu_2+\mu_3=0. \tag{19}$$

In cylindrical polar co-ordinates the equations of motion for no body forces acting on a non-Newtonian fluid in the steady state reduce to

$$\frac{\mu_1}{\rho}\left(\frac{\partial^2 u}{\partial r^2}+\frac{\partial^2 u}{\partial z^2}+\frac{1}{r}\frac{\partial u}{\partial r}-\frac{u}{r^2}\right)-\frac{1}{\rho}\frac{\partial p}{\partial r}=u\frac{\partial u}{\partial r}+w\frac{\partial u}{\partial z}-\frac{v^2}{r}-\frac{\mu_2 K_1}{\rho}-\frac{\mu_3 S_1}{\rho}, \tag{20}$$

$$\frac{\mu_1}{\rho}\left(\frac{\partial^2 v}{\partial r^2}+\frac{\partial^2 v}{\partial z^2}+\frac{1}{r}\frac{\partial v}{\partial r}-\frac{v}{r^2}\right)=u\frac{\partial v}{\partial r}+w\frac{\partial v}{\partial z}+\frac{uv}{r}-\frac{\mu_2 K_2}{\rho}-\frac{\mu_3 S_2}{\rho}, \tag{21}$$

$$\frac{\mu_1}{\rho}\left(\frac{\partial^2 w}{\partial r^2}+\frac{\partial^2 w}{\partial z^2}+\frac{1}{r}\frac{\partial w}{\partial r}\right)-\frac{1}{\rho}\frac{\partial p}{\partial z}=u\frac{\partial w}{\partial r}+w\frac{\partial w}{\partial z}-\frac{\mu_2 K_3}{\rho}-\frac{\mu_3 S_3}{\rho}, \tag{22}$$

where $(S_1, S_2, S_3)=\mathrm{div}((\mathbf{A}^{(1)})^2)$ and $(K_1, K_2, K_3)=\mathrm{div}(\mathbf{A}^{(2)})$.

We require to solve the equations (20)–(22) together with the continuity equation in both the geometries outlined in Sections 2 and 3. We again look for a series solution of these equations in powers of the angular velocity Ω. Now we note that (K_1, K_2, K_3) and (S_1, S_2, S_3) are quadratic in velocity and therefore if we only keep the first powers in Ω we obtain the same solution as for a

Newtonian fluid, i.e. equation (13) and its solution v_1 are independent of the non-Newtonian effects.

4.1. *Terms in* Ω^2

Since (K_1, K_2, K_3) and (S_1, S_2, S_3) are quadratic in velocity, we need only calculate the components of $\mathbf{A}^{(1)}$ and $\mathbf{A}^{(2)}$ for the case of $u=w=0$, $v=v_1$ which are given by Tidd *et al.*,[14] from which we obtain

$$\mu_2\mathbf{A}^{(2)}+\mu_3(\mathbf{A}^{(1)})^2=\mu_3\begin{bmatrix}0 & 0 & 0\\ 0 & \left(\dfrac{\partial v_1}{\partial r}-\dfrac{v_1}{r}\right)^2+\left(\dfrac{\partial v_1}{\partial z}\right)^2 & 0\\ 0 & 0 & 0\end{bmatrix}. \tag{23}$$

Hence keeping terms of Ω^2 equations (20)–(22) become

$$\frac{\mu_1}{\rho}\left(\frac{\partial^2 u_2}{\partial r^2}+\frac{\partial^2 u_2}{\partial z^2}+\frac{1}{r}\frac{\partial u_2}{\partial r}-\frac{u_2}{r^2}\right)-\frac{1}{\rho}\frac{\partial P_2}{\partial r}=-\frac{v_1^2}{r}+\frac{\mu_3}{\rho}\frac{1}{r}\left[\left(\frac{\partial v_1}{\partial r}-\frac{v_1}{r}\right)^2+\left(\frac{\partial v_1}{\partial z}\right)^2\right], \tag{24}$$

$$\frac{\mu_1}{\rho}\left(\frac{\partial^2 w_2}{\partial r^2}+\frac{\partial^2 w_2}{\partial z^2}+\frac{1}{r}\frac{\partial w_2}{\partial r}\right)-\frac{1}{\rho}\frac{\partial P_2}{\partial z}=0 \tag{25}$$

and the continuity equation, as before, becomes

$$\frac{\partial u_2}{\partial r}+\frac{u_2}{r}+\frac{\partial w_2}{\partial z}=0. \tag{26}$$

From (23) we may also see that the free surface conditions (1)–(3) for terms up to Ω^2 are unchanged from the Newtonian case. Hence non-Newtonian effects do not come into the free surface conditions using the perturbation analysis detailed here.

We non-dimensionalize the non-Newtonian model in an identical fashion to the Newtonian model using a length ratio $D=h/a$, a Reynolds number $Re=\rho\Omega a^2/\mu_1$, a surface tension parameter $S=T\rho a/\mu_1^2$ and a non-Newtonian parameter $N=\mu_3\Omega^2 a/T$. The results use values of $D=0{\cdot}1$, $Re=10{\cdot}0$, $S=300{\cdot}0$ and $N=\mu_3/27{\cdot}0$ for various choices of μ_3. Increasing μ_3 corresponds to the non-Newtonian effects becoming more important. We now outline our results for the two geometries.

4.2. *Parallel plates*

For this case we have an exact solution for v_1 given by (8). Using this, the right-hand side of equation (24) becomes

$$-r[L+z(K-L)/h]^2+(\mu_3 r/\rho)[(K-L)/h]^2. \tag{27}$$

We observe that the term in μ_3 of (27) is independent of z. Indeed this term (apart from a constant) is just that obtained by considering a Newtonian fluid between two parallel plates spinning at the same rate (i.e. $K=1$, $L=1$ in Section 2). In this case we have rigid body motion with $u=w=0$. Since the equations (24)–(26) are linear, we conclude that the flow pattern for the non-Newtonian fluid is the same as that already calculated for Newtonian fluids for all values of K and L. The free surface is also unchanged but the pressure will be different. These conclusions were also reached by Joseph.[6]

However, there are some difficulties in solving (24)–(26) numerically. The solution for a Newtonian fluid for the case $K = L$ does not produce values of u_2 and w_2 which are identically zero and, as we have seen, oscillate throughout the whole region. Thus even for a value of $\mu_3 = 1$ with $K \neq L$ the solution shows oscillations near $r = 0$ where the velocities are small, and for large μ_3, when the second term in (27) dominates, an oscillatory solution is obtained in the whole region.

4.3. *Cone and plate*

As noted in Section 3, no exact solution for v_1 can be easily found, so the right-hand-side terms of equation (24) have to be evaluated from the numerical solution of (5). We again evaluate the element contributions using a three-point Gaussian quadrature routine and input these into our finite element solver.

For element L3 erroneous results are found, particularly near the apex of the cone. The velocities have a non-physical checkerboard pattern on all the grids used. These results are a consequence of the lack of element mass balance and the fact that there is a pressure singularity at $r = 0$. The pressure distribution on the lower plate is proportional to $\log r$ for the case of an infinite cone and plate geometry.[22] However, for the locally mass-conserving element, element LC, this checkerboard pattern is not present and the solutions are seen to converge from one grid to the next.

The easiest way to see the non-Newtonian effect is to solve equations (24)–(26) keeping only the terms in μ_3 on the right-hand side of (24), i.e. solve (24)–(26) for an inertia-less non-Newtonian fluid between the cone and plate. Since the equations are linear, we may then add this solution to that already obtained for a Newtonian fluid in Section 3.

For values of $K = 1$ and $L = 0$ the non-Newtonian effect is to give two recirculations. The largest dominating recirculation is near the free surface and the fluid flows in the same direction as for a Newtonian fluid. The weaker recirculation has flow in the opposite direction and is located near the centreline. The flow pattern for this case is illustrated in Figure 12. On adding the two solutions together, the two recirculations remain with the dominating one made stronger and the weaker one reduced. Large velocity gradients are present near the free surface and the associated free surface displacement is over twice as large as that of the corresponding Newtonian fluid. Increasing the value of μ_3 has the effect of increasing the dominance of the non-Newtonian terms. A point is reached where the Newtonian terms can be ignored. The streamlines for the case

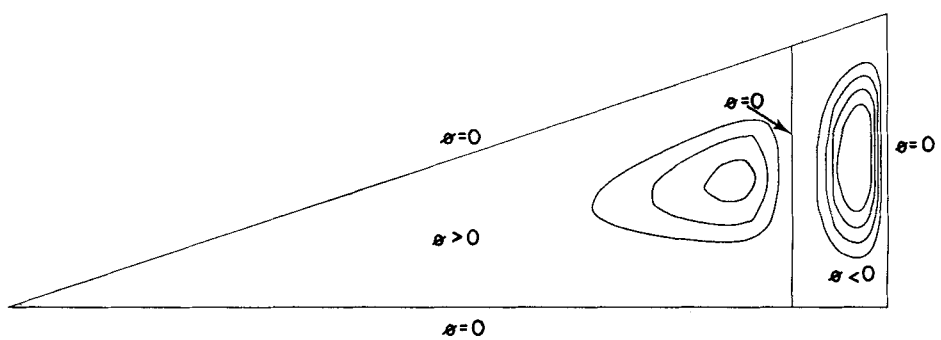

Figure 12. Cone and plate streamlines for an inertia-less non-Newtonian fluid with $K = 1$, $L = 0$ and $\mu_3 = 1$. Contour values: 0·3E-5, 0·25E-5, 0·2E-5, 0·0, −0·49E-5, −0·74E-5, −0·99E-5, −0·12E-4

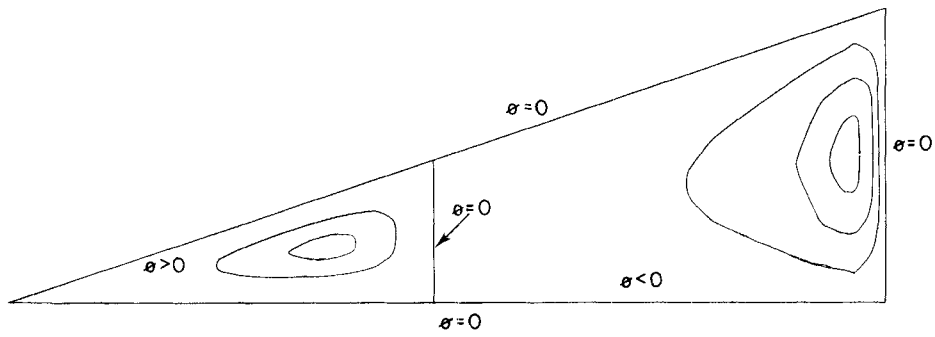

Figure 13. Cone and plate streamlines for non-Newtonian fluid with $K=1$, $L=0$, $Re=10$ and $\mu_3=1$. Contour values: 0·1E-6, 0·6E-7, 0·0, −0·5E-5, −0·17E-4, −0·29E-4

$\mu_3=1{\cdot}0$ are illustrated in Figure 13 and should be compared with the single recirculation obtained for a Newtonian fluid in Figure 11.

Changing the value of L with $K=1$ does not alter the general flow pattern of an inertia-less non-Newtonian fluid, which still shows two recirculations. However, different flow patterns will be obtained on adding the non-Newtonian effect to the respective Newtonian solutions of Section 3 provided μ_3 is sufficiently small.

4. CONCLUSIONS

In this paper we have calculated flow patterns and free surface shapes for Newtonian and non-Newtonian fluids confined between both parallel plates and a cone and plate configuration at low Reynolds number. The importance of this work is in applications to rheology, where devices of the form described here with a stationary plate and a rotating cone or plate (i.e. $K=1$, $L=0$) are used to measure viscosity and normal stress differences.

In all the calculations that we have done it has been assumed that the free surface can be considered as a perturbation from the vertical circular cylinder. The full Navier–Stokes equations have been solved by Tidd *et al.*[23,25] with the free surface calculated using a trial free boundary approach and iterating on the normal stress condition (3). On comparing the results with those presented here, it is concluded that the perturbation technique is accurate up to Reynolds numbers of 100 with a surface tension parameter of $S=300$. The relation between Reynolds number and surface tension is important since it determines when the trial free boundary method diverges. The stability analysis for rigidly rotating captive drops by Ungar and Brown[26] and by Brown and Scriven[27] is important in this respect.

For a non-Newtonian fluid an assumption of a slowly moving fluid was made for the constitutive equation and the results are calculated by a linearized approach similar to that of the Navier–Stokes equations. These results will only be valid for small perturbations of the free surface from the vertical circular cylinder. The secondary flow patterns in the cone–plate geometry are consistent with the known results for a cone rotating in a sea of fluid.[5] The nature and sense of rotation are seen to depend dramatically on the elastic properties of the fluid. This perturbation technique has also been used in the situation of a cone–plate bounded by a cylinder.[23] In this case a further secondary flow reversal is predicted, which is an affect observed by Hoppmann and Baronet.[28]

All the results have been calculated using triangular finite elements with quadratic velocities and linear pressures. It was found that continuous linear pressures produced non-physical velocity solutions in certain circumstances. Using ideas suggested by Griffiths,[17] a new locally mass-conserving element overcame these difficulties. The stability of the finite element calculations for Stokes flow is equivalent to the satisfaction of the Babuska–Brezzi condition.[20] It is well known that element L3 is stable and Thatcher and Silvester[19] have recently shown that element LC also satisfies the Babuska–Brezzi condition.

ACKNOWLEDGEMENT

D.M.T. would like to acknowledge the financial support given by the SERC during the production of this report.

REFERENCES

1. M. Holodniok, M. Kubícek and V. Hlavácek, 'Computation of the flow between two rotating coaxial disks', *J. Fluid Mech.*, **81,** 689–699 (1977).
2. H. P. Pao, 'A numerical computation of a confined rotating flow', *Trans. ASME E: J. Appl. Mech.*, **37,** 480–487 (1970).
3. D. Dijkstra and G. J. F. van Heijst, 'The flow between two finite rotating disks enclosed by a cylinder', *J. Fluid Mech.*, **128,** 123–154 (1983).
4. D. B. Cox, 'Radial flow in the cone-plate viscometer', *Nature*, **193,** 670 (1962).
5. K. Walters, *Rheometry*, Chapman and Hall, 1975.
6. D. D. Joseph, 'Slow motion and viscometric motion: stability and bifurcation of the rest state of a simple fluid', *Arch. Rat. Mech. Anal.*, **56,** 99–157 (1974).
7. G. M. Harriott and R. A. Brown, 'Flow in a differentially rotated cylindrical drop at low Reynolds number', *J. Fluid Mech.*, **126,** 269–285 (1983).
8. R. I. Tanner, R. E. Nickell and R. W. Bilger, 'Finite element methods for the solution of some incompressible non-Newtonian fluid mechanics problems with free surfaces', *Comput. Methods Appl. Mech. Eng.*, **6,** 155–174 (1975).
9. K. J. Ruschak and L. E. Scriven, 'Rimming flow of liquid in a rotating horizontal cylinder', *J. Fluid Mech.*, **76,** 113–125 (1976).
10. F. M. Orr and L. E. Scriven, 'Rimming flow: numerical simulation of steady, viscous, free surface flow with surface tension', *J. Fluid Mech.*, **84,** 145–165 (1978).
11. J. M. Hyun, 'Flow in an open tank with a free surface driven by the spinning bottom', *Trans. ASME J. Fluid. Eng.*, **107,** 495–499 (1985).
12. R. Keunings, 'An algorithm for the simulation of transient viscoelastic flows with free surfaces', *J. Comput. Phys.*, **62,** 199–220 (1986).
13. C. Taylor and P. Hood, 'A numerical solution of the Navier–Stokes equations using the Finite Element method', *Comput. Fluids*, **1,** 73–100 (1973).
14. D. M. Tidd, R. W. Thatcher and A. Kaye, 'The free surface flow of Newtonian and non-Newtonian fluids trapped by surface tension', *Numerical Analysis Report No. 127*, Manchester University/UMIST, 1986.
15. C. Taylor and T. G. Hughes, *Finite Element Programming of the Navier–Stokes Equations*, Pineridge Press, 1981.
16. R. Teman, *Navier–Stokes Equations*, North-Holland, Amsterdam, 1977.
17. D. F. Griffiths, 'The effect of pressure approximations on finite element calculations of incompressible flows', in K. W. Morton and M. J. Baines (eds), *Numerical Methods for Fluid Dynamics*, Academic Press, 1982.
18. P. M. Gresho, R. L. Lee, S. T. Chan and J. M. Leone, 'A new finite element for incompressible or Boussinesq fluids', in *Proc. Third Int. Conf. on Finite Elements in Flow Problems*, Wiley, 1980.
19. R. W. Thatcher and D. J. Silvester, 'A locally mass conserving quadratic velocity linear pressure element', *Numerical Analysis Report No. 147*, Manchester University/UMIST, 1987.
20. V. Girault and P.-A. Raviart, *Finite Element Methods for Navier–Stokes Equations*, Springer-Verlag, 1986.
21. D. J. Silvester, *Ph.D. Thesis*, UMIST, 1984.
22. A. Kaye, *D.Phil. Thesis*, University of Oxford, 1965.
23. D. M. Tidd, *Ph.D. Thesis*, UMIST, 1987.
24. R. B. Bird, R. C. Armstrong and O. Hassager, *Dynamics of Polymeric Liquids, Volume 1: Fluid Mechanics*, Wiley, 1977.
25. D. M. Tidd, R. W. Thatcher and A. Kaye, 'The free surface in parallel-plate and cone–plate viscometers', in C. Taylor, W. G. Habashi and M. M. Hafez (eds), *Laminar and Turbulent Flow*, Pineridge Press, 1987.
26. L. H. Ungar and R. A. Brown, 'The dependence of the shape and stability of captive rotating drops on multiple parameters', *Phil. Trans. Roy. Soc. Lond. A*, **306,** 347–370 (1982).
27. R. A. Brown and L. E. Scriven, 'The shape and stability of rotating captive drops', *Phil. Trans. Roy. Soc. Lond. A*, **297,** 51–79 (1980).
28. W. H. Hoppmann and C. N. Baronet, 'Study of flow induced in viscoelastic liquid by a rotating cone', *Trans. Soc. Rheol.*, **9,** 417–423 (1965).